Annuaire de l'Université de Sofia "St. Kliment Ohridski", Faculté de Physique, 96, 2003

MAGNETIC FIELD- AND FORCE-DISTRIBUTION IN SUPERCONDUCTING MAGNETS

CECO DUSHKIN, MASAYOSHI NAWA*, TOMA FUJITA*, SEICHIRO NAKABAYASHI*

Department of General and Inorganic Chemistry, Faculty of Chemistry
**Faculty of Science, Saitama University, Japan*

Цецо Душкин, Масайоши Нава, Тома Фуджита, Сейичиро Накабаяши. РАЗПРЕДЕЛЕНИЕ НА МАГНИТНОТО ПОЛЕ И СИЛА В СВРЪХПРОВОДНИКОВИ МАГНИТИ

Силното магнитно поле, създадено в отвора на комерсиален свръхпроводников магнит, е с нарастващо приложение в левитацията на обекти и обработката на материали. Тук ние пресмятаме пространствените разпределения на магнитното поле и сила, допускайки единичен дебел соленоид с ефективна геометрия и физични параметри, задаващи същото поле както комерсиалния магнит с неизнестна и доста комплицирана конструкция. Радиалната зависимост е намерена като степенно развитие с коефициенти производните на функцията на централното поле спрямо аксиалната координата. Предложената теория е потвърдена с експериментални данни за два свръхпроводящи магнита с максимални магнитни полета 10 T и 4 T и съответни диаметри на отвора 15 cm и 40 cm. Детайлните карти на магнитното поле позволяват предсказване на зоната за стабилна левитация на диамагнитни обекти. Общата валидност на теоретичния подход е демонстрирана като прости правила за дизайна на свръхпроводникови соленоиди по отношение на ширината и максимума на разпределението на полето и на силата.

Ceco Dushkin, Masayoshi Nawa, Toma Fujita, Seichiro Nakabayashi. MAGNETIC FIELD- AND FORCE-DISTRIBUTION IN SUPERCONDUCTING MAGNETS

High magnetic field created in the bore of a commercial superconducting magnet is of increasing application in levitation of objects and materials processing. Here we calculate the space distributions of the magnetic field and force assuming single thick solenoid of effective geometry and physical parameters providing the same field as the commercial magnet of unknown or rather complicated construction. The radial dependence is obtained as power series with coefficients the derivatives of the central-field function with respect to the axial coordinate. The proposed theory is verified with experimental data for two superconducting magnets of maximum magnetic fields 10 T and 4 T and and 40 cm, respectively. The detailed maps of the magnetic field allow predicting the zone for stable levitation of diamagnetic objects. The general validity of the theoretical approach is demonstrated as simple rules for the design of superconducting solenoids with respect to the width and maximum of the field distribution and the force strength.

Keywords: superconducting magnet, solenoid, magnetic field, levitation, magnetic materials

PACS number: 85.25.L, 85.70.R, 07.55.Db, 75.20, 75.50

INTRODUCTION

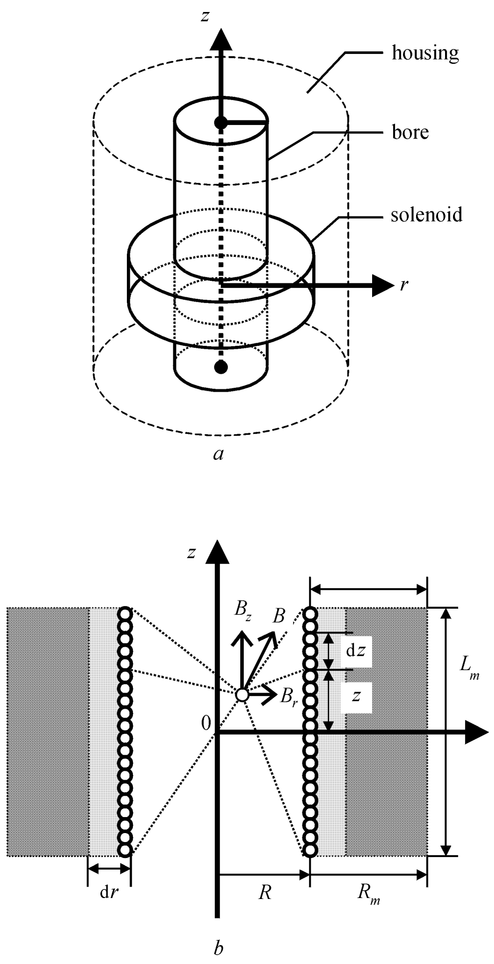

Fig. 1

Superconducting magnets are used in practice, where high magnetic field is required: processing of inorganic [1–7] and organic [7] materials, leveling of liquids [8–11], separation processes [12–15], plasma technology [16,17], biology [18], electrochemistry [19,20], ordering of colloidal dispersions [21,22], etc. Most of these processes are carried out with diamagnetic objects captured in the zone of stable levitation in the upper part of magnet (Fig. 1), where the magnetic force counterbalances the gravity force [23–30]. The magnetic force applied on an object varies with the spatial distribution of the magnetic field $\boldsymbol{B}(\boldsymbol{r})$ depending on the construction of the most crucial part of the magnet: the superconducting solenoid.

The solenoid part can be composed of one (single-coil solenoid [19]) or more coils (compound solenoid [31–36]). A superconducting coil comprises a number of unit coils (filaments, wire coils) wound on a bobbin and covered by a copper plate for heat exchange upon cooling [32, 33]. A composite solenoid consists of two or more coils of different filament material of the unit coils and geometrical dimensions. For two-coils s olenoid a good combination seems NbTi as the filaments wound on aluminum bobbin (outer coil) and Ni_3Sn as the filament material wound on stainless steel (inner coil). Single-coil solenoid is used in wide-bore magnets of moderate field, for example bore diameter $\Phi = 30$ cm and nominal field at the magnet center $B_0^0 = 5$ T [34]. The two-coil solenoid generates high magnetic field in relatively narrow bore ($B_0^0 = 10$ T, $\Phi = 10$ cm) [34]. The increase in the number of coils aims either increasing the nominal field in the hybrid magnets [37–41] or creating a zone of constant magnetic force [42, 43] for special applications such as the growth of protein crystals [8–11]. The hybrid magnet, dedicated for total field more than 30 T, has outer superconducting magnet of nominal field 10–15 T and inset (resistive magnet) of 10–20 T. The inset is either superconducting solenoid or Bitter magnet with conductor plates of copper composite material separated by insulator and cooled by water flowing along channels in the plates.

Due to complexity of magnet construction, the actual field inside the bore can be either numerically calculated [35, 36, 43, 44] (only the manufacturer knows all constructive parameters) or experimentally measured [45]. One numerical method expands the central magnetic field in power series of Legendre polynomials with coefficients determined by the optimal design of multiple coils [44]. Numerical examples for the field, $B(r,z)$, and the magnetic force density, $f(r,z)$, are rarely available as contour maps $z(r)$ at equidistant B or f [35, 36, 43]. They are convenient only for plotting the central field $B_0(z) = B(0,z)$ and force density $f(0,z) = B_0\,\mathrm{d}B_0/\,\mathrm{d}z$. The need of numerical differentiation of $B_0(z)$ restricts the calculation of the force and, hence, the experimentation. For example, the complex motion of droplets [23] or colloidal dispersions [21, 22] requires detailed knowledge for the axial and radial dependence of force along the magnet bore. From similar obstacles suffers the study of dynamic processes [4–6, 8–11, 15–17], which may become practical if a transparent picture of the magnetic field and force distribution was available.

The purpose of our paper is to express the magnetic field components as functions of the coordinates taking the central magnetic field and the dimensions of the superconducting solenoid as parameters.

The new points of our approach are:

i) Expressing the radial field component and the radial dependence of the axial field component in a circular solenoid.

ii) Deriving equations for the radial and axial magnetic force components.

iii) Description of the field in real superconducting magnets.

The new insights of paper are stemming from the detailed knowledge of the mathematical functions describing the field and force in a magnet, which have been determined until now only numerically. They allow formulating the simple rules of the superconducting solenoid design.

EXPERIMENT

We used two superconducting magnets with parameters shown in Table 1. One is JMTD-10T150 of Japan Magnet Technology (JMT) with vertical bore of diameter $\Phi = 15$ cm and length $L = 100$ cm. The other one is TM-4V40 of Toshiba, also vertical, of bore parameters $\Phi = 40$ cm and $L = 50$ cm, respectively. The magnetic field $\boldsymbol{B}$ in the bore is directed to the top of magnet decreasing along the z-axis from the center to bore ends – see Figs. 2a, 3a, 5 and 6a. The maximum field, $B_0^0 = 10$ T, is at the magnet center located $L_1 = 64.1$ cm from the bore top for JMTD-10T150 and at $L_1 = 25$ cm for TM-4V40.

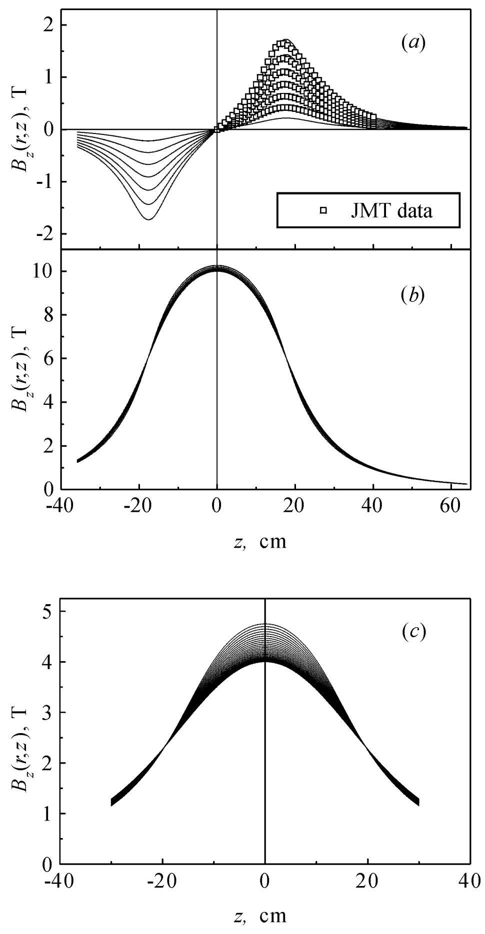

Fig. 2

We measured the magnetic field distribution, $B(r, z)$, in the bore of JMTD-10T150 with Gauss meter (Lake Shore, model 421). The Gauss meter had an axial type probe of special design: diameter 6.3 mm and length 910 mm. Only the axial component of the magnetic flux density was measured at the probe tip. The data points in one scan were collected at each 5 millimeters, moving in z-direction from the bore center to the upper and lower ends, consequently. To map the radial field dependence, eight scans were done all together at intervals of 1 cm starting from $r = 0$ and ending at $r = 7$ cm (the bore radius is $R = 7.5$ cm). Our experimental data were not sufficient for complete description of magnetic field. For example, it was not possible to measure the radial field component, B_r, in JMTD-10T150 with the same accuracy as B_z. That is why we used also data provided by the manufacturers of magnets denoted as JMT data and Toshiba data.

The data for $B_z(r, z)$, plotted in Fig. 2*b* for JMTD-10T150, do not differ so much for different r; nevertheless, the radial field gradient increases from the bore center to the periphery. More pronounced is the radial dependence of B_z for TM-4V40—up to 1 T difference at the maximum in Fig. 2*c* (due also to larger r). Since $\partial B_z/\partial r$ enters the expression for force density, the radial field non-uniformity appreciably contributes for both magnets, especially close to the bore periphery.

Contribution to the magnetic force has also the radial field component $B_r(r, z)$, which has maxima as a function of z, increasing in value with increasing r (Fig. 2*a*). The maxima, located at positive z in the zone of stable levitation, contribute to the total force. Minima of B_r should be observed at negative z as shown by

Table 1. Parameters of the superconducting magnets

No	Magnet Model, Manufacturer	B_0^0, T	Φ, cm	L, cm	L_1, cm	L_m, cm	H_m, cm	R_m, cm	$\widetilde{B}_0$, T	Δz, cm
1.	10T-200 [36], Kawasaki Heavy Industries	10	20	130	35	44	22	32	6.86	44.8
2.	JMTD-10T150 [12], Japan Magnet Technology	10	15	100	64.1	35	17.7	25	6.77	35.6
3.	TM-4V40, Toshiba	4	40	50	25	24	12	32	4.72	31.8
4.	HF-10-100VHT [31], Sumitomo Heavy Industries	10	10	100	35	22	11	16	6.86	22.4
5.	7T High-T$_c$ [37] Sumitomo Electric Industries	7	5	50	25	19	14.5	17	3.23	19.2
6.	High field magnet [3],	8	10	70		16	8	13	5.95	16.6
7.	Spectromag 1000 [38], Oxford Instruments	8	5	47	20	15	20	22.5	2.68	15.4

the calculations (no data available). Similar effect of B_r is numerically shown on contour plots for the magnetic force [35, 36, 42].

The data points $\mathrm{d}^n B_0/\,\mathrm{d}z^n$ (Figs. 3*b*–*e*; 4*b*–*e*) are numerical differentiations of the data for $B_0(z)$ in Figs. 3*a* and 4*a*, respectively. They are further used to adjust the model parameters, H_m and L_m (unknown for the devices) by minimizing the deviation of the data points from the respective theoretical values $\mathrm{d}^n B_0/\,\mathrm{d}z^n$ in the Appendix. Up to four derivatives of $B_0(z)$ figure out in the expressions for magnetic force density—see below. Therefore, the minimization has been simultaneously carried out for B_0 and B_0'. For JMTD-10T150, the mean square deviations are 0.33 T and 0.0038 T/cm, respectively (typical also for the other magnets). These values lead to expectedly pronounced differences in the fits for higher-order derivatives: 0.0061 T/cm^2 (B_0''), 0.0016 T/cm^3 (B_0''') and 0.0014 T/cm^4 (B_0^{IV}). Signs “prime”, “second”, “third” and “forth” denote the respective derivatives of $B_0(z)$ on z. The derivatives for the two magnets, JMTD-10T150 and TM-4V40, look rather different, comparing Figs. 3*c* with 4*c* (B_0''), 3*d* with 4*d* (B_0''') and 3*e* with 4*e* (B_0^{IV}). This difference is coming from the slight bending in the central portion of in Fig. 3*b*, missing in the counter-figure Fig. 4*b*. Such tiny effects, coming from the construction of particular magnets, can also influence the magnetic force.

THEORY

The cylindrical solenoid in Fig. 1 is an oversimplified model of the real counterpart: i) The solenoid comprises only the superconducting coils occupying a space of effective geometry close to that of the real solenoid of unknown parameters; ii) One coil of one type superconductor wire creates in the bore the same magnetic field $B(r, z)$ as the real solenoid; the latter may consist of more coils of

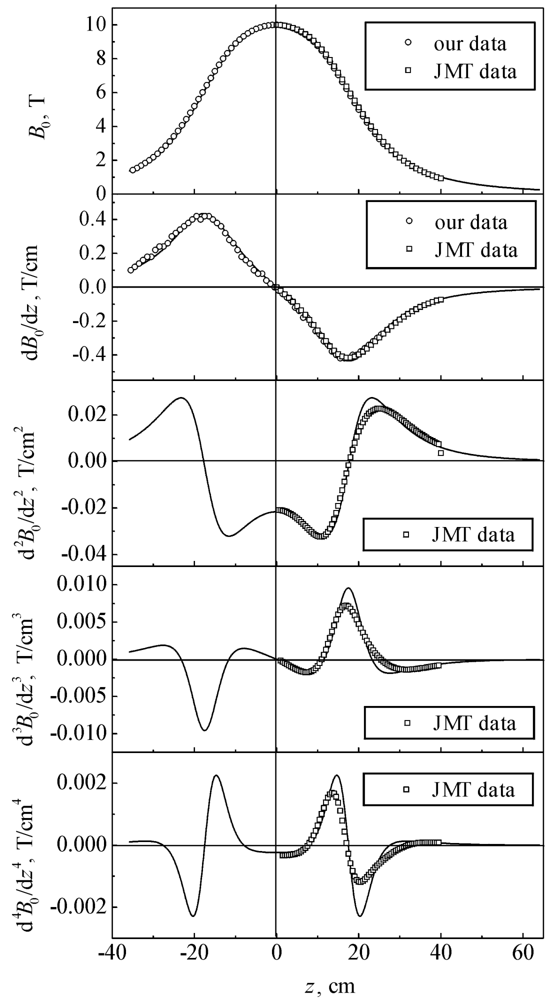

Fig. 3

different wire types; iii) The inner solenoid radius is equal to the bore radius, R, provided by the manufacturer, while the outer solenoid radius, R_m, and length, L_m, are adjustable parameters to fit the experimental data. For a compound solenoid, Rm should be close to the outer radius of the outermost coil, whereas L_m is likely to be an average of the coil lengths; iv) The model solenoid of thickness $H_m = R_m - R$ is referred to as a thick solenoid. (H_m should be close to the sum of thicknesses of concentric coils). In the thin-solenoid limit, H_m tends to zero to give known results [27, 30]. (A thin solenoid will be referred to as the wire monolayer shown by circles in Fig. 1b of known field. For the purpose of solution, a thin solenoid is considered also the elementary layer of thickness dr comprising several wire monolayers superimposing their fields).

The radial dependence of the axial field B_z can be derived from the experiments by noting that the deviation from the central field $B_0(z)$ is a small quantity, depending on r^2. Then one can write:

$$B_z(r, z) = B_0(z) + b(z)r^2. \tag{1}$$

The function $b(z)$ in Eq. (1) is calculated from the data in Fig. 2b, c. Plotted in Fig. 4, it is symmetrical and obeys the condition $b(0) = b_0$. Comparison with Figs. 3c and 4c reveals the similarity of $-b(z)$ and B_0'' quantified below. Close to the bore wall ($r \sim R$) higher order terms on r^2 should also be taken into account.

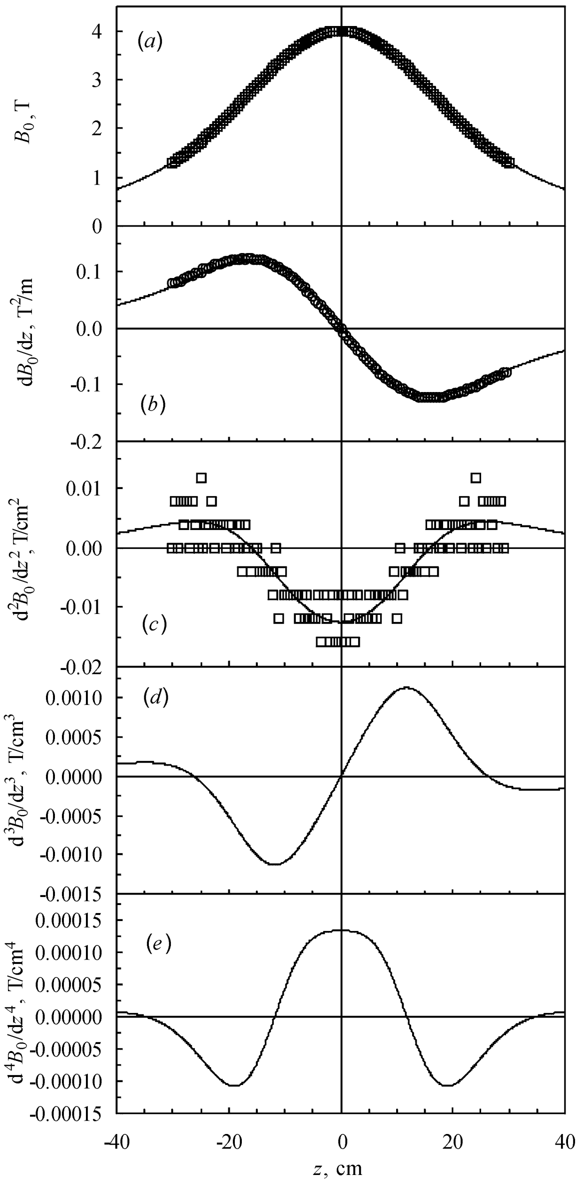

(a)
B_0, T
4
3
2
1
0
0.1
0.0
-0.1
-0.2
dB_0/dz, T^2/m
(b)
0.01
0.00
-0.01
-0.02
d^2B_0/dz^2 T/cm^2
(c)
(d)
0.0010
0.0005
0.0000
-0.0005
-0.0010
-0.0015
d^3B_0/dz^3, T/cm^3
(e)
0.00015
0.00010
0.00005
0.00000
-0.00005
-0.00010
-0.00015
d^4B_0/dz^4, T/cm^4
-40
-20
0
20
40
z, cm

Fig. 4

The central magnetic field $B_0(z) = B_z(0,z)$ in Eq. (1) is that for a thick solenoid [46, 47]:

$$\beta_0(\zeta) = (1+\zeta)\ln\frac{\widetilde{\rho}+\sqrt{(1+\zeta)^2+\widetilde{\rho}}}{\rho+\sqrt{(1+\zeta)^2+\rho}} + (1-\zeta)\ln\frac{\widetilde{\rho}+\sqrt{(1-\zeta)^2+\widetilde{\rho}}}{\rho+\sqrt{(1-\zeta)^2+\rho}}. \qquad (2)$$

$\beta_0 = B_0/\widetilde{B}_0$ is dimensionless quantity; $\widetilde{B}_0 = \mu_0 IN/4H_m$ is the characteristic field; $\mu_0 = 4\pi\times10^{-7}$ N/A^2 is permeability of the vacuum (in SI units); I is the electric current; $N = N_L N_H$ is the total number of wire coils (N_L is the number of wire coils in a layer; N_H is the number of layers in a coil, Fig. 1b); $\zeta = z/(L_m/2)$; $\rho = R/(L_m/2)$; $\widetilde{\rho} = R_m/(L_m/2)$. At $z = 0$ one obtains from Eq. (2)

$$B_0^0 = \frac{\mu_o IN}{2H_m}\ln\frac{\widetilde{\rho}+\sqrt{1+\widetilde{\rho}^2}}{\rho+\sqrt{1+\rho^2}}. \qquad (3)$$

$B_0(z)$ is a symmetrical function of z confirmed by the experimental data for solenoids, $B_0(-z) = B_0(z)$.

From Eq. (2) one obtains the derivatives of $B_0(z)$ necessary in other calculations—Appendix. For JMTD-10T150, B_0', has a minimum at $z^+ = 17.8$ cm and a maximum of the same absolute value at $z^- = -17.8$ cm—Fig. 3b. For TM-4V40 (Fig. 4b), the respective values are $z\pm = \pm15.9$ cm. Hence, B_0' is an odd function, $B_0'(-z) = -B_0'(z)$ with $B_0''(z^\pm) = 0$. In analogy with B_0 and B_0', the even derivatives are symmetrical functions of z, while the odd derivatives are asymmetrical.

Knowing $B_z(r,z)$, Eqs. (1) and (2), the radial field $B_r(r,z)$ follows from the continuity equation $\nabla\boldsymbol{B} = 0$, where $\nabla = [(1/r)(\partial/\partial r)r, \partial/\partial z]$. Replacing here Eq. (1) and integrating from 0 to r, one obtains

$$B_r(r,z) = -\frac{\mathrm{d}^2B_0}{\mathrm{d}z^2}\frac{r}{2} + \frac{\mathrm{d}b}{\mathrm{d}z}\frac{r^3}{4}. \qquad (4)$$

B_Φ is assumed zero. Eqs. (1) and (4) can be regarded as series expansions of the central field $B_0(z)$. From the symmetry of B_z, the first perturbation term will be $B_0''r^2/4$, hence the function $b(z)$ turns out to be

$$b(z) = -\frac{1}{4}\frac{\mathrm{d}^2B_0}{\mathrm{d}z^2}. \qquad (5)$$

The plots in Fig. 5 experimentally confirm Eq. (5).

The magnetic force $\boldsymbol{F}$ in a medium of constant magnetic susceptibility χ is [43]

$$\boldsymbol{F} = \frac{\chi}{\mu_0}\int_V \nabla\boldsymbol{B}\cdot\boldsymbol{B}\,\mathrm{d}\nu. \qquad (6)$$

The integration is over the volume of medium V. The product $\nabla\boldsymbol{B}\cdot\boldsymbol{B} = (f_r, f_z)$ is considered vectorial force field with components $f_r = B_r\dfrac{\partial B_r}{\partial r} + B_z\dfrac{\partial B_z}{\partial r}$ and

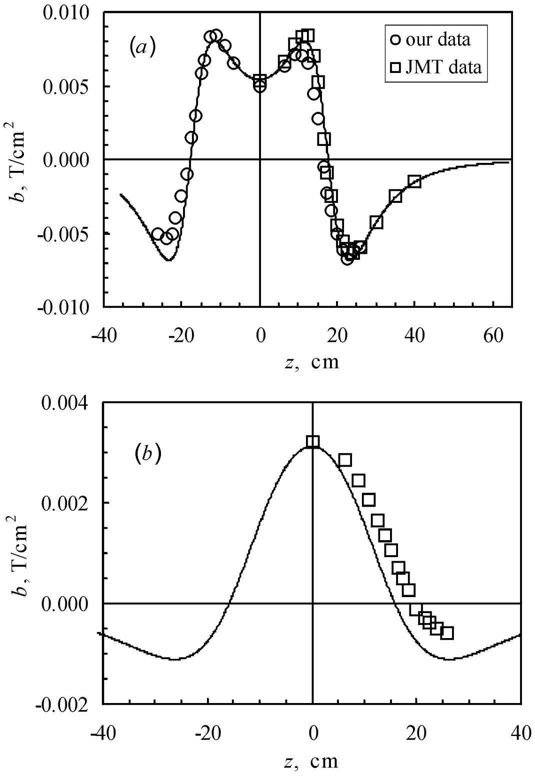

Fig. 5

$f_z = B_r \dfrac{\partial B_r}{\partial z} + B_z \dfrac{\partial B_z}{\partial z}$. The force per unit volume f is then called magnetic force density. In view of Eq. (6) the components become

$$f_r = \left(-\frac{B_0' r}{2} + \frac{B_0''' r^3}{16}\right)\left(-\frac{B_0'}{2} + \frac{3B_0''' r^2}{16}\right) + \left(B_0 - \frac{B_0'' r^2}{4}\left(-\frac{B_0'' r}{2}\right)\right), \qquad (7)$$

$$f_z = \left(-\frac{B_0' r}{2} + \frac{B_0''' r^3}{16}\right)\left(-\frac{B_0''}{2} + \frac{3B_0^{IV} r^3}{16}\right) + \left(B_0 - \frac{B_0'' r^2}{4}\left(B_0' \frac{-B_0''' r^2}{4}\right)\right). \qquad (8)$$

In the simplest case, neglecting all derivatives higher than first, one gets from Eqs. (7) and (8) $f_r = 0$ and

$$f_z = B_0 \frac{\mathrm{d}B_0}{\mathrm{d}z}. \qquad (9)$$

Replaced in Eq. (6), they yield the magnetic force used in the literature: $F_z = (\chi V/\mu_0) B_0 B_0'$.

RESULTS

The 3D-plots in Fig. 6 are based on Eqs. (1) and (4) with parameters derived from the experimental data in Figs. 2, 3 and 4. The component $B_z(r,z)$ seems rather uniform with r. The radial one, $B_r(r,z)$, is of appreciably high magnitude in the zones of function extrema. Important for the levitation of diamagnetic objects is the zone between $z = 14.9$ and 19.6 cm for JMTD-10T150 [23]. This affects also the magnetic force magnitude. The contour plots of the slices $B_{r,z} = \mathrm{const}$ resemble very much the respective map for B for another magnet of the same series—JMTD-12T100M [36] (at $B \approx B_z$).

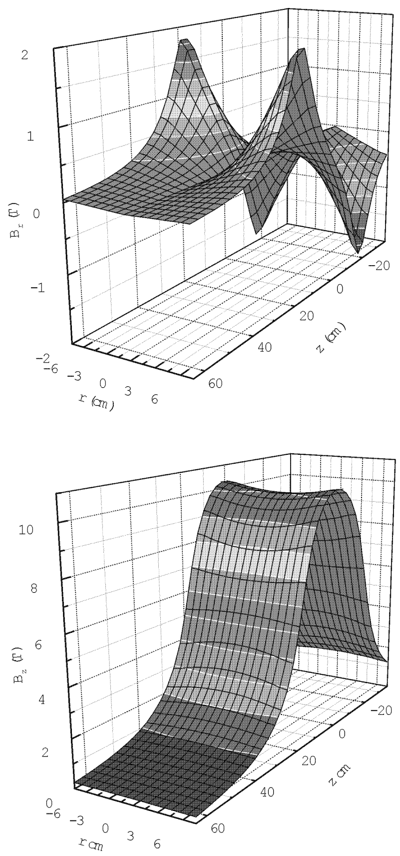

Fig. 6

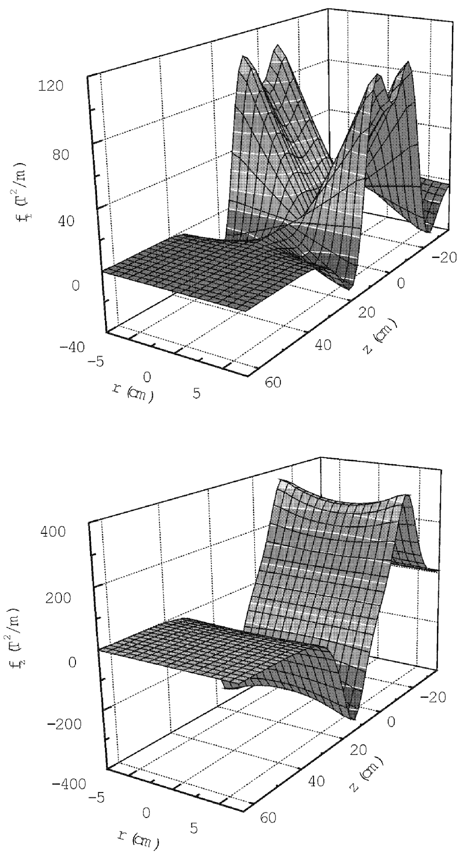

Fig. 7

The 3D-forces are seen in Fig. 7 for JMTD-10T150. The contour plots resemble very much that for another superconducting magnet from the same series, JMTD-12T100M [36]. Being of higher nominal field $B_0^0 = 12$ T, it creates bigger force: f_r up to -200 T^2/m and f_z up to -600 T^2/m at positive z.

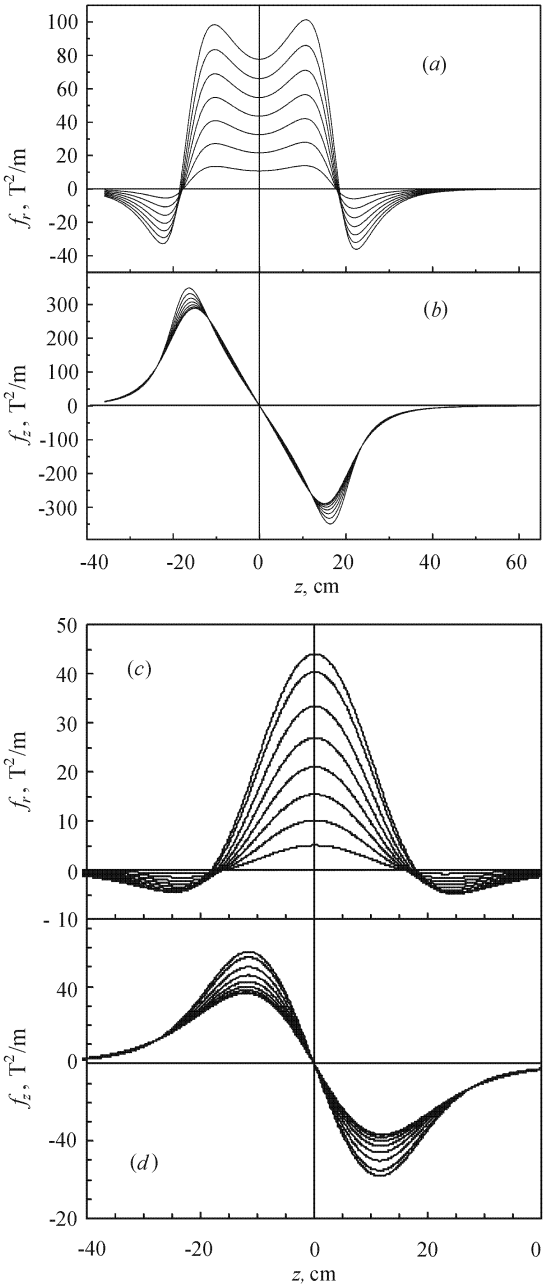
(a)
(b)
(c)
(d)
f_r, T^2/m
f_z, T^2/m
z, cm
100
80
60
40
20
0
-20
-40
300
200
100
-100
-200
-300
-40
-20
0
20
40
60
50
30
10
- 10

Fig. 8

Fig. 8a plots the radial force, f_r, in JMTD-10T150. The minimum fr at $z = 0$ separates two asymmetrical maxima; their difference is more pronounced at $r = 7.5$ cm. The negative values have two minima, also slightly different. In the levitation zone, f_r changes sign at $z = 18.5$ cm. In diamagnetic medium, it will direct the respective force component F_r from the bore center to the periphery at $z > 18.5$ cm and oppositely at $z < 18.5$ cm.

In contrast, the radial force for TM-4V40 exhibits only one maximum at $z = 0$ in Fig. 8c with the positive force twice as small compared to that in 8a. The two minima are also asymmetrical. The crossing points of f_r with the abscissa are symmetrical, but change from $z = \pm 15.9$ cm at $r = 2$ cm to $z = \pm 18$ cm at $r = 15$ cm.

The plots of axial force, f_z, in Figs. 8b and 8d are of similar trends as the respective first derivatives in Figs. 3b and 4b. The leading term $B_0\,\mathrm{d}B_0/\,\mathrm{d}z$ determines the force at $r = 0$. f_z is an odd function with a maximum and a minimum, $f_z(r, -z) = f_z(r, z)$.

DISCUSSION

Here we generalize the features of JMTD-10T150 and TM-4V40 for other magnets considered in literature. The purpose is to find simple rules for the construction of superconducting magnets, which explain the influence of solenoid geometry and material on the maximum magnetic field, B_0^0, and magnetic force, $B_0\,\mathrm{d}B_0/\,\mathrm{d}z$. Commercially available magnets turn out to have common features reflecting the manufacture school and dedication to rather general use, including in scientific laboratories. From consideration are excluded very high field magnets ($B_0^0 > 10$ T) [14, 42] due to the complexity of their design and the lack of reference data for B_0^0 and $B_0\,\mathrm{d}B_0/\,\mathrm{d}z$.

All magnets from Table 1 follow very well the model predictions seen from Fig. 9, which represents the respective functions, calculated from experimental data. The fits use two parameters, the solenoid length Lm and solenoid thickness H_m (Fig. 1b), using the rest from the literature. As in Figs. 3 and 4, the parameters have been adjusted in simultaneous fits of the data for $B_0(z)$ and its derivatives (usually the first and rarely the second due to scattering of the data after numerical differentiation)—cf. Fig. 6c. All magnets have second derivative of the same type as in Fig. 3c, except TM-4V40, due probably to the too large bore diameter ($\Phi = 40$ cm). In many cases, the theoretical curves are almost undistinguishable from the experimental data (for clarity not shown in Fig. 9).

The parameters L_m and H_m seem effective quantities representing the length and width of the model solenoid creating the same field and force distribution in the magnet as the real solenoid(s), whose construction remains more or less unknown from the manufacturers. Nevertheless, the calculated parameters are close to those reported for similar devices. For example, a prototype of magnet of $B_0^0 = 10$ T and $\Phi = 10$ cm (JMT) [33] has two concentric solenoids of total effective width

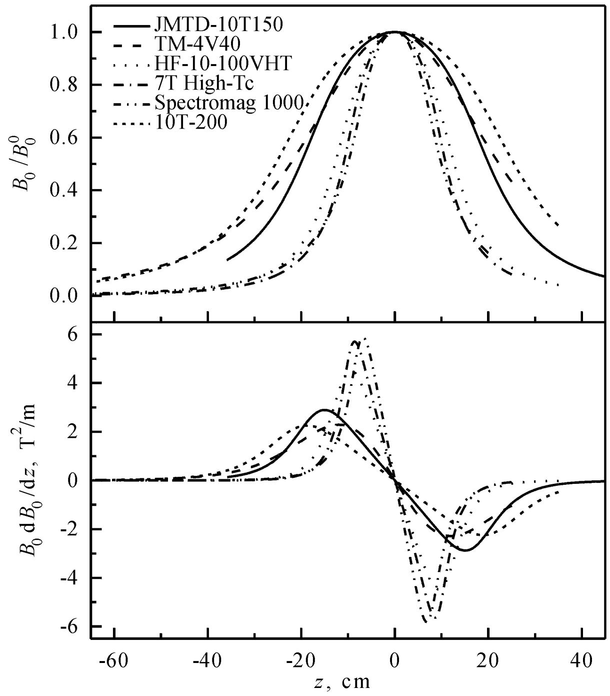

Fig. 9

$H_m \approx 8$ cm and average length $L_m \approx 24.5$ cm. Similarly, one of the models of Toshiba ($B_0^0 = 10$ T, $\Phi = 10$ cm, two coils) [32] is of average parameters $H_m \approx 7$ cm and $L_m \approx 21.5$ cm, respectively.

The magnets can be divided into two main groups: those creating a broad field distribution in Fig. 9a, coupled to respective weak force in Fig. 9b, and those of a narrow distribution and large force. It turns out that these two quantities depend in different ways on the magnet geometry. Relevant measure for the distribution width is the difference between the two symmetrical inflection points of $B_0(z)$, corresponding also to the two extrema of B_0'. It can be readily estimated from the two zeros of B_0'' at $z^{\pm}$ as $\Delta z = z^{+} - z^{-}$. The peak width Δz is plotted in Fig. 10a versus the solenoid length L_m. The straight line drawn at slope unity shows that

$$\Delta z = L_m \tag{10}$$

within the experimental error. This striking result is mathematically coming from the derivation of Eq. (2), obtained after integration in the limits of solenoid. Therefore, the function $B_0(z)$ and derivatives will have peculiarities at the solenoid ends.

Practically, Eq. (10) states the first empirical rule of magnet design:

I. To spread the magnetic field on a larger area inside the magnet one needs

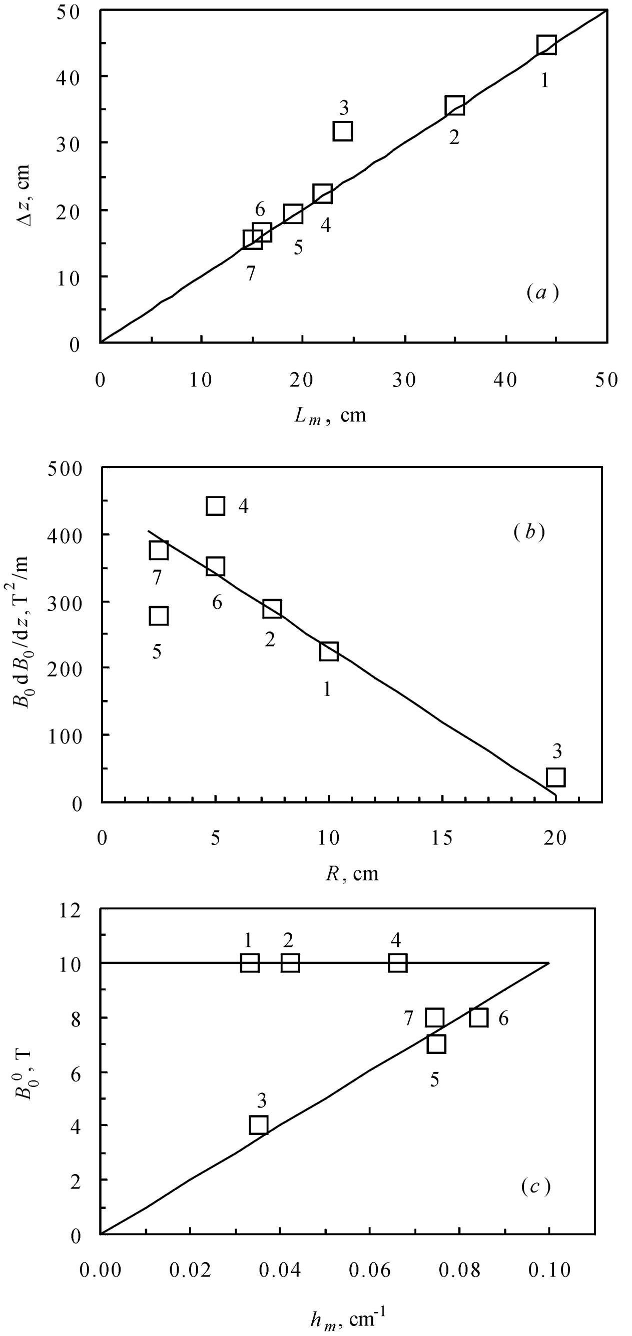
50
40
30
20
10
0
0
10
20
30
40
50
Δz, cm
L_m, cm
1
2
3
4
5
6
7
(a)
500
400
300
200
100
0
0
5
10
15
20
$B_0\,dB_0/dz$, T^2/m
R, cm
4
7
6
5
2
1
3
(b)
12
10
8
6
4
2
0
0.00
0.02
0.04
0.06
0.08
0.10
B_0^0, T
h_m, cm^{-1}
1
2
4
7
6
5
3
(c)

Fig. 10

longer solenoid. Rule I is not obvious, since L_m is substantially smaller than the total bore length L in many cases. For this reason, the solenoid length was chosen as the primary parameter of listing the magnets in Table 1. The deviation of point 3 from Eq. (11) is due to very large bore diameter of TM-4V40.

It is known that magnets of smaller bore diameter, $\Phi = 2R$, give stronger magnetic force. Fig. 10*b* proves this fact by plotting the maximum values of the curves from Fig. 9*b*, $B_0\,\mathrm{d}B_0/\,\mathrm{d}z|_{\max} = |B_0\,\mathrm{d}B_0/\,\mathrm{d}z|$, taken at the function maximum or minimum. The data points obey linear relationship on the radius:

$$B_0\frac{\mathrm{d}B_0}{\mathrm{d}z}\Big|_{\max} = 450 - 22R\infty. \tag{11}$$

Equation (11) represents the second rule of magnet design:

II. To get larger magnetic force one needs solenoid of smaller internal radius. Again, rule II is not obvious, because the manufacturer provides the room temperature bore radius, which is always smaller than R. The thin bore solenoid ($R \to 0$) gives a limit, 450 T^2/m, for the force generated by the commercial magnets considered here. Note that even solenoid No. 4, which positively deviates from Eq. (11), does not exceed this limit.

The most important parameter for any magnet is its nominal field B_0^0 taken in the magnet center at the maximum allowed current $I_{\max}$ (the field provided by the manufacturer—Table 1). At smaller current I, B_0^0 should be reduced by a linear coefficient: 0.129 T/A for JMTD-10T150 and 0.046 T/A for TM-4V40. Such a decrease will further reflect the space distribution of the magnetic field in accord with Eq. (2). Although the direct field measurements were always at maximum B00, experiments on levitation of objects at varying B_0^0 [23] showed that, over a broad space domain, the functional dependence remains essentially the same.

The prediction of B_0^0 is complicated because, according to Eq. (3), it depends on both the solenoid geometry and the material: maximum allowed current and number of conductors in the coil(s). For magnets in one series the respective plots [12, 36] show $B_0^0 \sim 1/R\dfrac{n!}{r!(n-r)!}$, where R states for the bore radius. Magnets of different series obey different curves [36]. We propose more general representation, inspired from Eq. (3), by introducing the quantity

$$h_m = \frac{1}{H_m}\ln\frac{\widetilde{\rho} + \sqrt{1+\widetilde{\rho}^2}}{\rho + \sqrt{1+\rho^2}}. \tag{12}$$

h_m can be considered as the reverse solenoid thickness reduced by other geometrical parameters. Then Eq. (3) simply reads

$$B_0^0 = \frac{\mu_0 IN}{2}h_m, \tag{13}$$

where the contributions of geometry (h_m) and material (IN) are clearly separated.

Equation (13) thus represents the third rule of magnet design:

III. At constant product IN, one can achieve bigger nominal field B_0^0 by properly increasing the quantity h_m.

The plots in Fig. 10c show two examples for application of this rule. The straight line, increasing with h_m, is of slope $\mu_0 IN/2 = 1$ T m. The horizontal line of $B_0^0 = 10$ T at increasing hm means that the product IN is correspondingly decreased. For example, by decreasing the current I or the conductor number N.

The typical values of N shown in Table 2 are calculated by Eq. (3) for the specified current $I_{\max}$. To estimate the crossection area of one conductor, we divided by N the crossection area of the coil, $L_m H_m$, multiplied by the filling factor 0.6046 for hexagonal close packing of the conductors. Assuming a circular conductor of diameter d_m, the values in the table were obtained. They are close to the respective diameters of NbTi conductors in other JMT magnets (0.85–0.95 mm at the upper limit) [34] and to d_m for NbTi and Nb3Sn in magnets of TOSHIBA (0.9 and 0.96) [32]. Despite of the good coincidence, the conductor diameters in Table 2 should be considered as effective quantities possibly averaged over the two coils composing a solenoid.

Table 2. Material parameters of magnets

Magnet model	$I_{\max}$, A	N	$L_m H_m$, cm^2	d_m, mm
JMTD-10T150	77.452	48724	612.5	0.98
TM-4V40	87	20729	288	1.03

The zone of stable levitation is defined [27, 30] as the area where two functions,

$$D_\nu = B_0 B_0'' + {B_0'}^2 \frac{n!}{r!(n-r)!} \tag{14}$$

for vertical stability, and

$$D_h = {B_0'}^2 - 2B_0 B_0'' \tag{15}$$

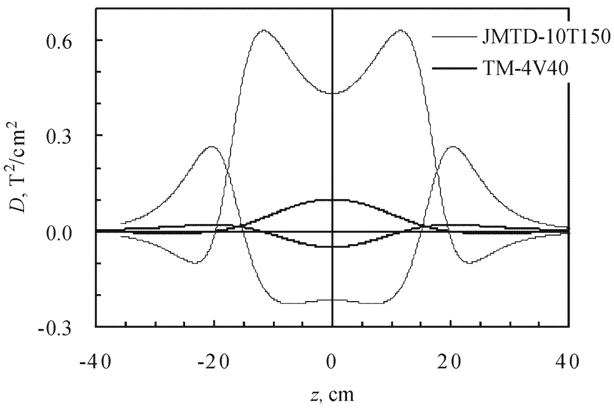

Fig. 11

for horizontal stability are simultaneously positive (Fig. 11). There are two symmetrical zones at negative and positive z.

Table 3. Zone of stable levitation for diamagnetic objects

No	Magnet model	$z_{\min}$, cm	$z_{\max}$, cm	ΔZ, cm	$L_m/2$, cm
1.	10T-200	18.9	24.9	6.0	22.0
2.	JMTD-10T150	14.9	19.7	4.8	17.5
3.	TM-4V40	12.1	19.7	7.6	12.0
4.	HF-10-100VHT	9.5	12.4	2.9	11.0
5.	7T High-T_c	8.7	10.1	1.4	9.5
6.	Magnet	6.8	9.5	2.7	8.0
7.	Spectromag 1000	6.9	8.1	1.2	7.5

Important for the stable levitation of diamagnetic objects is the zone at $z > 0$, shown in Table 3 for the magnets in this study. $z_{\min}$ is the lower boundary of the zone, $z_{\max}$—the upper boundary, $\Delta Z = z_{\max} - z_{\min}$ is the zone width. With decreasing the solenoid length, L_m, the levitation zone is obviously shrinking. The upper boundary of the zone, $z_{\max}$, always exceeds the upper end of the solenoid, shown as the half-length $L_m/2$.

CONCLUSION

A new theoretical approach is calculating the magnetic field and force in superconducting magnet modeled as a single solenoid of effective length and width. The model parameters and function coefficients are determined from comparison with experimental data for two different superconducting magnets.

Based on the treatment simple rules for the design of magnet solenoids have been formulated: First, the width of magnetic field distribution, taken between the two inflection points of the function, is equal to the solenoid length. Second, the strength of the magnetic force, defined as the magnitude of the function maximum (or minimum), increases linearly with decreasing of the inner solenoid radius. Third, the maximum field at the magnet center can be changed by properly varying the solenoid geometry or the physical properties such as the current and the conductor number.

The predicted zone of stable levitation in vertically situated magnet generally decreases with the solenoid length with the upper zone boundary located higher than the solenoid end.

ACKNOWLEDGEMENT

The financial support of the RFTF (Research for the Future) program of the Japan Society for Promotion of Science is gratefully acknowledged. The authors

thank to Japan Magnet Technology Inc. and Toshiba for kindly provided data about their superconducting magnets.

APPENDIX

Two limits of Eqs. (2) and (3), necessary for the calculations, are considered: First, for thin coil solenoid [27] the limit $H_m \to 0$ ($R = R_m$, $\rho = \widetilde{\rho}$) [48] transforms Eq. (2) into

$$\beta_0(\zeta) = \frac{(1+\zeta)}{\sqrt{(1+\zeta)^2+\rho^2}} + \frac{(1-\zeta)}{\sqrt{(1-\zeta)^2+\rho^2}}. \tag{A1}$$

Separately differentiating in Eq. (3) the nominator and denominator on Hm and then taking the limit resolves the uncertainty of 0/0 [48] gives ($N_H = 1$ and $N = N_L$)

$$B_0^0 = \frac{\mu_0 I N_L}{2L\sqrt{1+\rho^2}}. \tag{A2}$$

Second, for thin bore solenoid, $\rho \to 0$ ($R \ll L_m$, $\widetilde{\rho} \to \chi$) Eqs. (2) and (3) give respectively:

$$\beta_0 = (1+\zeta)\ln\frac{\chi+\sqrt{(1+\zeta)^2+\chi^2}}{(1+\zeta)} + (1-\zeta)\ln\frac{\chi+\sqrt{(1-\zeta)^2+\chi^2}}{(1-\zeta)}, \tag{A3}$$

$$B_0^0 = \frac{\mu_0 I N}{2H_m}\ln(\chi+\sqrt{1+\chi^2}). \tag{A4}$$

$\chi = H_m/(L_m/2)$. Due to the finite solenoid thickness, H_m, Eqs. (6) and (7) cannot be deduced in the frames of the thin-coil approximation [27].

Below are listed the derivatives of Eq. (2) important for the computations.

First derivative:

$$\begin{aligned}\frac{\mathrm{d}\beta_0}{\mathrm{d}\zeta} &= \ln\frac{[\widetilde{\rho}+\sqrt{(1+\zeta)^2+\widetilde{\rho}^2}][\rho+\sqrt{(1-\zeta)^2+\rho^2}]}{[\rho+\sqrt{(1+\zeta)^2+\rho^2}][\widetilde{\rho}+\sqrt{(1-\zeta)^2+\widetilde{\rho}^2}]}\\ &+(1+\zeta^2)\left\{\frac{1}{\sqrt{(1+\zeta^2)+\widetilde{\rho}}[\widetilde{\rho}+\sqrt{(1+\zeta^2)+\widetilde{\rho}}]}-\frac{1}{\sqrt{(1+\zeta^2)+\rho}[\rho+\sqrt{(1+\zeta^2)+\rho}]}\right\}\\ &-(1-\zeta)^2\left\{\frac{1}{\sqrt{(1-\zeta^2)+\widetilde{\rho}}[\widetilde{\rho}+\sqrt{(1-\zeta^2)+\widetilde{\rho}}]}-\frac{1}{\sqrt{(1-\zeta^2)+\rho}[\rho+\sqrt{(1-\zeta^2)+\rho}]}\right\}.\end{aligned} \tag{A5}$$

Second derivative:

$$
\begin{aligned}
\frac{\mathrm{d}^2\beta_0}{\mathrm{d}\zeta^2} = 3(1+\zeta)\Bigg\{ & \frac{1}{\sqrt{(1+\zeta)^2+\widetilde{\rho}}[\widetilde{\rho}+\sqrt{(1+\zeta)^2+\widetilde{\rho}}]} \\
& - \frac{1}{\sqrt{(1+\zeta)^2+\rho}[\rho+\sqrt{(1+\zeta)^2+\rho}]}\Bigg\} \\
& + 3(1-\zeta)\Bigg\{\frac{1}{\sqrt{(1-\zeta)^2+\widetilde{\rho}}[\widetilde{\rho}+\sqrt{(1-\zeta)^2+\widetilde{\rho}}]} \\
& - \frac{1}{\sqrt{(1-\zeta)^2+\rho}[\rho+\sqrt{(1-\zeta)^2+\rho}]}\Bigg\} \\
& + (1+\zeta)^3\Bigg\{-\frac{\widetilde{\rho}+2\sqrt{(1+\zeta)^2+\widetilde{\rho}^2}}{[(1+\zeta)^2+\widetilde{\rho}^2]^{3/2}[\widetilde{\rho}+\sqrt{(1+\zeta)^2+\widetilde{\rho}^2}]^2}+ \\
& \frac{\rho+2\sqrt{(1+\zeta)^2+\rho^2}}{[(1+\zeta)^2+\rho^2]^{3/2}[\rho+\sqrt{(1+\zeta)^2+\rho^2}]^2}\Bigg\} \\
& - (1-\zeta)^3\Bigg\{-\frac{\widetilde{\rho}+2\sqrt{(1-\zeta)^2+\widetilde{\rho}^2}}{[(1-\zeta)^2+\widetilde{\rho}^2]^{3/2}[\widetilde{\rho}+\sqrt{(1-\zeta)^2+\widetilde{\rho}^2}]^2}+ \\
& \frac{\rho+2\sqrt{(1-\zeta)^2+\rho^2}}{[(1-\zeta)^2+\rho^2]^{3/2}[\rho+\sqrt{(1-\zeta)^2+\rho^2}]^2}\Bigg\}.
\end{aligned}
\tag{A6}
$$

Third derivative:

$$
\begin{aligned}
\frac{\mathrm{d}^3\beta_0}{\mathrm{d}\zeta^3} = 3\Bigg\{ & \frac{1}{\sqrt{(1+\zeta)^2+\widetilde{\rho}^2}[\widetilde{\rho}+\sqrt{(1+\zeta)^2+\widetilde{\rho}^2}]} - \\
& \frac{1}{\sqrt{(1+\zeta)^2+\rho^2}[\rho+\sqrt{(1+\zeta)^2+\rho^2}]} \\
& - \frac{1}{\sqrt{(1-\zeta)^2+\widetilde{\rho}^2}[\widetilde{\rho}+\sqrt{(1-\zeta)^2+\widetilde{\rho}^2}]} - \\
& \frac{1}{\sqrt{(1-\zeta)^2+\rho^2}[\rho+\sqrt{(1-\zeta)^2+\rho^2}]}\Bigg\}
\end{aligned}
\tag{A7}
$$

$$
\begin{aligned}
&+6(1+\zeta)^2\left\{\frac{\widetilde{\rho}+2\sqrt{(1+\zeta)^2+\widetilde{\rho}}}{[(1+\zeta)^2+\widetilde{\rho}^2]^{3/2}[\widetilde{\rho}+\sqrt{(1+\zeta)^2+\widetilde{\rho}}]}\right.\\
&\qquad\left.-\frac{\rho+2\sqrt{(1+\zeta)^2+\rho^2}}{[(1+\zeta)^2+\rho^2]^{3/2}[\rho+\sqrt{(1+\zeta)^2+\rho}]}\right\}\\
&+(1-\zeta)^2\left\{-\frac{\widetilde{\rho}+2\sqrt{(1-\zeta)^2+\widetilde{\rho}}}{[(1-\zeta)^2+\widetilde{\rho}^2]^{3/2}[\widetilde{\rho}+\sqrt{(1-\zeta)^2+\widetilde{\rho}}]}\right.\\
&\qquad\left.-\frac{\rho+2\sqrt{(1-\zeta)^2+\rho^2}}{[(1-\zeta)^2+\rho^2]^{3/2}[\rho+\sqrt{(1-\zeta)^2+\rho}]}\right\}\\
&+(1+\zeta)^4\left\{\frac{11\widetilde{\rho}^2+9\widetilde{\rho}\sqrt{(1+\zeta)^2+\widetilde{\rho}^2}+8(1+\zeta)^2}{[(1+\zeta)^2+\widetilde{\rho}^2]^{5/2}[\widetilde{\rho}+\sqrt{(1+\zeta)^2+\widetilde{\rho}^2}]^3}\right.\\
&\qquad\left.-\frac{11\rho^2+9\rho\sqrt{(1+\zeta)^2+\rho^2}+8(1+\zeta)^2}{[(1+\zeta)^2+\rho^2]^{5/2}[\rho+\sqrt{(1+\zeta)^2+\rho^2}]^3}\right\}\\
&-(1-\zeta)^4\left\{\frac{11\widetilde{\rho}^2+9\widetilde{\rho}\sqrt{(1-\zeta)^2+\widetilde{\rho}^2}+8(1-\zeta)^2}{[(1-\zeta)^2+\widetilde{\rho}^2]^{5/2}[\widetilde{\rho}+\sqrt{(1-\zeta)^2+\widetilde{\rho}^2}]^3}\right.\\
&\qquad\left.-\frac{11\rho^2+9\rho\sqrt{(1-\zeta)^2+\rho^2}+8(1-\zeta)^2}{[(1-\zeta)^2+\rho^2]^{5/2}[\rho+\sqrt{(1-\zeta)^2+\rho^2}]^3}\right\}.
\end{aligned}
\tag{A7}
$$

Fourth derivative:

$$
\begin{aligned}
\frac{\mathrm{d}^4\beta_0}{\mathrm{d}\zeta^4}={}&15(1+\zeta)\left\{-\frac{\widetilde{\rho}+2\sqrt{(1+\zeta)^2+\widetilde{\rho}^2}}{[(1+\zeta)^2+\widetilde{\rho}^2]^{3/2}[\widetilde{\rho}+\sqrt{(1+\zeta)^2+\widetilde{\rho}^2}]^2}\right.\\
&\qquad\left.+\frac{\rho+2\sqrt{(1+\zeta)^2+\rho^2}}{[(1+\zeta)^2+\rho^2]^{3/2}[\rho+\sqrt{(1+\zeta)^2+\rho^2}]^2}\right\}\\
&-15(1-\zeta)\left\{\frac{\widetilde{\rho}+2\sqrt{(1-\zeta)^2+\widetilde{\rho}^2}}{[(1-\zeta)^2+\widetilde{\rho}^2]^{3/2}[\widetilde{\rho}+\sqrt{(1-\zeta)^2+\widetilde{\rho}^2}]^2}\right.\\
&\qquad\left.-\frac{\rho+2\sqrt{(1-\zeta)^2+\rho^2}}{[(1-\zeta)^2+\rho^2]^{3/2}[\rho+\sqrt{(1-\zeta)^2+\rho^2}]^2}\right\}
\end{aligned}
\tag{A8}
$$

$$
\begin{aligned}
&+(1+\zeta)^3\left\{\frac{11\widetilde{\rho}^2+9\widetilde{\rho}\sqrt{(1+\zeta)^2+\widetilde{\rho}^2}+8(1+\zeta)^2}{[(1+\zeta)^2+\widetilde{\rho}^2]^{5/2}[\widetilde{\rho}+\sqrt{(1+\zeta)^2+\widetilde{\rho}^2}]^3}\right.\\
&\qquad\left.-\frac{11\rho^2+9\rho\sqrt{(1+\zeta)^2+\rho^2}+8(1+\zeta)^2}{[(1+\zeta)^2+\rho^2]^{5/2}[\rho+\sqrt{(1+\zeta)^2+\rho^2}]^3}\right\}\\
&+(1-\zeta)^3\left\{\frac{11\widetilde{\rho}^2+9\widetilde{\rho}\sqrt{(1-\zeta)^2+\widetilde{\rho}^2}+8(1-\zeta)^2}{[(1-\zeta)^2+\widetilde{\rho}^2]^{5/2}[\widetilde{\rho}+\sqrt{(1-\zeta)^2+\widetilde{\rho}^2}]^3}\right.\\
&\qquad\left.-\frac{11\rho^2+9\rho\sqrt{(1-\zeta)^2+\rho^2}+8(1-\zeta)^2}{[(1-\zeta)^2+\rho^2]^{5/2}[\rho+\sqrt{(1-\zeta)^2+\rho^2}]^3}\right\}\\
&+(1+\zeta)^5\left\{-\frac{102\widetilde{\rho}^3+108\widetilde{\rho}^2\sqrt{(1+\zeta)^2+\widetilde{\rho}^2}+87\widetilde{\rho}(1+\zeta)^2}{[(1+\zeta)^2+\widetilde{\rho}^2]^{7/2}[\widetilde{\rho}+\sqrt{(1+\zeta)^2+\widetilde{\rho}^2}]^4}\right.\\
&\qquad-\frac{+48(1+\zeta)^2\sqrt{(1+\zeta)^2+\widetilde{\rho}^2}}{[(1+\zeta)^2+\widetilde{\rho}^2]^{7/2}[\widetilde{\rho}+\sqrt{(1+\zeta)^2+\widetilde{\rho}^2}]^4}\\
&\left.+\frac{102\rho^3+108\rho^2\sqrt{(1+\zeta)^2+\rho^2}+87\rho(1+\zeta)^2+48(1+\zeta)^2\sqrt{(1+\zeta)^2+\rho^2}}{[(1+\zeta)^2+\rho^2]^{7/2}[\rho+\sqrt{(1+\zeta)^2+\rho^2}]^4}\right\}\\
&+(1-\zeta)^5\left\{-\frac{102\widetilde{\rho}^3+108\widetilde{\rho}^2\sqrt{(1-\zeta)^2+\widetilde{\rho}^2}+87\widetilde{\rho}(1-\zeta)^2}{[(1-\zeta)^2+\widetilde{\rho}^2]^{7/2}[\widetilde{\rho}+\sqrt{(1-\zeta)^2+\widetilde{\rho}^2}]^4}\right.\\
&\qquad-\frac{+48(1-\zeta)^2\sqrt{(1-\zeta)^2+\widetilde{\rho}^2}}{[(1-\zeta)^2+\widetilde{\rho}^2]^{7/2}[\widetilde{\rho}+\sqrt{(1-\zeta)^2+\widetilde{\rho}^2}]^4}\\
&\left.+\frac{102\rho^3+108\rho^2\sqrt{(1-\zeta)^2+\rho^2}+87\rho(1-\zeta)^2+48(1-\zeta)^2\sqrt{(1-\zeta)^2+\rho^2}}{[(1-\zeta)^2+\rho^2]^{7/2}[\rho+\sqrt{(1-\zeta)^2+\rho^2}]^4}\right\}.
\end{aligned}
\tag{A8}
$$

REFERENCES

1. Braithwaite, D., E. Beaugnon, R. Tournier. *Nature (London)*, **354**, 1991, 134.
2. Michaud, B., E. Beaugnon, A. Sulpice, R. Tournier, J. Claverie. *Mater. Trans. JIM*, **41**, 2000, 962.
3. Gaucherand, F., E. Beaugnon. *Physica B*, **294-295**, 2001, 96.
4. Yamamoto, I., M. Yamaguchi, M. Fujino, F. Ishikawa, T. Goto, S. Miura. *Physica B*, **216**, 1996, 399.
5. Kakimoto, K., K.-W. Yi. *Physica B*, **216**, 1996, 406.
6. Motokawa, M., M. Hamai, T. Sato, I. Mogi, S. Awaji, K. Watanabe, N. Kitamura, M. Makihara. *Physica B*, **294-295**, 2001, 729.
7. Ueno, S., M. Iwasaka. *J. Appl. Phys.*, **75**, 1994, 7177.

8. Ataka, M., S. Sakurazawa, T. Kubota, N. Wakayama, T. Kiyoshi, H. Wada. In: Proceedings of the 1999 International Symposium on New Magneto-Science, Omiya, Japan, JSTC, Kawaguchi, 1999, 123.
9. Motokawa, M. In: Proceedings of the 1999 International Symposium on New Magneto-Science, Omiya, Japan, JSTC, Kawaguchi, 1999, 181.
10. Kimura, T. In: Proceedings of the 1999 International Symposium on New Magneto-Science, Omiya, Japan, JSTC, Kawaguchi, 1999, 193.
11. Ozeki, S., Y. Kojima, T. Ishii, K. Iguchi, Y. Imai, K. Tajima, I. Mogi, K. Watanabe, H. Abe. In: Proceedings of the 1999 International Symposium on New Magneto-Science, Omiya, Japan, JSTC, Kawaguchi, 1999, 553.
12. Burgoyne, J. W., In: Proceedings of the 1999 International Symposium on New Magneto-Science, Omiya, Japan, JSTC, Kawaguchi, 1999, 71.
13. Ikezoe, Y., T. Kaihatsu, T. Suetsuna, H. Uetake, N. Hirota, K. Kitazawa, In: Proceedings of the 1999 International Symposium on New Magneto-Science, Omiya, Japan, JSTC, Kawaguchi, 1999, 401.
14. Brooks, J. S., J. A. Cothern. *Physica B*, **294-295**, 2001, 721.
15. Sato, N., G. Uchida, T. Kaneko, S. Shimizu, S. Iizuka. *Phys. Plasmas*, **8**, 2001. 1786.
16. Shoda, M. *Physica B*, **216**, 1996, 409.
17. Hirota, N., J. Nakagawa, K. Kitazawa. *J. Appl. Phys.*, **85**, 1999, 5717.
18. Mogi, I. *Physica B*, **216**, 1996, 406.
19. Nakabayashi, S., K. Inokuma, A. Karantonis. *Phys. Rev. E*, **59**, 1999, 6599.
20. Nakabayashi, S., R. Aogaki, A. Karantonis, U. Iguchi, K. Ushida, M. Nawa. *J. Electroanal. Chem.*, **473**, 1999, 54.
21. Fujita, T., S. Nakabayashi, In: Proceedings of the 2000 International Symposium on New Magneto-Science, Omiya, Japan, JSTC, Kawaguchi, 2000, 421 (Japanese).
22. Nawa, M., R. Baba, S. Nakabayashi, In: Proceedings of the 2000 International Symposium on New Magneto-Science, Omiya, Japan, JSTC, Kawaguchi, 2000, 427 (Japanese).
23. Fujita, T., C. Dushkin, M. Nawa, S. Nakabayashi. *Chem. Lett.*, 2001, 992.
24. Beaugnon, E., R. Tournier. *Nature (London)*, **349**, 1991, 470.
25. Beaugnon, E., D. Fabregue, D. Billy, J. Nappa, R. Tournier. *Physica B*, **294-295**, 2001, 715.
26. Vailert, M. A., D. L. Whitaker, H. J. Maris, G. M. Seidel. Phys. *Rev. Lett.*, **77**, 1996, 4840.
27. Berry, M. V., A. K. Geim. *Eur. J. Phys.*, **18**, 1997, 307.
28. Ikezoe, Y., N. Hirota, J. Nakagawa, K. Kitazawa. *Nature (London)*, **393**, 1998, 749.
29. Kitazawa, K., Y. Ikezoe, H. Uetake, N. Hirota. *Physica B*, **294-295**, 2001, 709.
30. Simon, M. D., A. K. Geim. *J. Appl. Phys.*, **87**, 2000, 6200.
31. Brown, F. J., N. W. Kerley, R. B. Knox, K. W. Timms. *Physica B*, **216**, 1996, 203.
32. Urata, M., K. Koyanagi, T. Kuriyama, K. Yamamoto, S. Nakayama, T. Yazawa, S. Nomura, Y. Yamada, H. Nakagome, S. Murase, H. Maeda, O. Horigami. *Physica B*, **216**, 1996, 209.
33. Shibutani, K., S. Itoh, T. Takagi, O. Ozaki, R. Hirose, S. Hayashi, M. Shimada, R. Ogawa, Y. Kawate, Y. Inoue, K. Matsumoto, N. Kimura. In: Proceedings of the 1996 International Cryogenic Engineering Conference and International Cryogenic Mate als Conference, Kitakyushu, Japan, Elsevier, 1996, 1129.
34. Shibutani, K., S. Itoh, O. Ozaki, T. Takagi, T. Miyazaki, R. Hirose, S. Hayashi, M. Shimada, R. Ogawa, Y. Kawate, K. Matsumoto, N. Kimura, K. Takabatake. In: Proceedings of the 1997 Cryogenic Engineering Conference and International Cryogenic terials Conference, Portland, USA, paper HE2.
35. Koyanagi, K., T. Asano, S. Matsumoto, T. Kiyoshi, H. Wada. In: Proceedings of the 1999 International Symposium on New Magneto-Science, Omiya, Japan, JSTC, Kawaguchi, 1999, 580.
36. Kamikado, T., K. Shibutani. In: Proceedings of the 1999 International Symposium on New Magneto-Science, Omiya, Japan, JSTC, Kawaguchi, 1999, 586.
37. Maeda, H., K. Inoue, T. Kiyoshi, T. Asano, Y. Sakai, T. Takeuchi, K. Itoh, H. Aoki, G. Kido. *Physica B*, **216**, 1996, 141.
38. Gao, B. J., J. L. Chen, S. L. Yuan, W. F. Yuan, F. T. Wang, L. R. Ding, X. N. Liu, Z. M.Liu, Z. Huang, Z. Y. Chen, S. Wang. *Physica B*, **216**, 1996, 166.

39. Iwasa, Y. *Physica B*, **216**, 1996, 186.
40. Bird, M. D., S. Bole, Y. M. Eyssa, B. J. Gao, H.-J. Schneider-Muntau. *Physica B*, **216**, 1996, 193.
41. Murase, S., S. Nakayama, Y. Wachi, T. Fujioka, S. Hanai, N. Aoki, M. Uchihara, M. Hakamata, K. Noguchi, N. Shiga, K. Inoue, T. Takeuchi, K. Itoh, T. Kiyoshi, H. Maeda. *Physica B*, **216**, 1996, 233.
42. Kiyoshi, T., T. Asano, S. Matsumoto, O. Ozaki, K. Koyanagi, H. Nakayama, J. Fujihara, H. Wada, In: Proceedings of the 1999 International Symposium on New Magneto-Science, Omiya, Japan, JSTC, Kawaguchi, 1999, 77.
43. Ozaki, O., T. Kiyoshi, S. Matsumoto, H. Wada, K. Koyanagi, J. Fujihara, H. Nakayama, In: Proceedings of the 1999 International Symposium on New Magneto-Science, Omiya, Japan, JSTC, Kawaguchi, 1999, 568.
44. Noguchi, S., A. Ishiyama. *Physica B*, **216**, 1996, 212.
45. Nakabayashi, S., R. Aogaki, U. Iguchi, M. Nawa. *Chem. Lett.*, 1998, 591.
46. Golden, L. B., J. R. Klein, L. Tongson. *Am. J. Phys.*, **56**, 1988, 846.
47. Dushkin, C., M. Nawa, T. Fujita, S. Nakabayashi. *J. Appl. Phys.*, **91**, 2002, 10212.
48. Bronstein, I. N., K. A. Semendyaev. Handbook of Mathematics. Moscow, Nauka, 1986 (in Russian).

Received June 2003

Ceco Dushkin
St. Kliment Ohridski University of Sofia
Faculty of Chemistry
Department of General and Inorganic Chemistry
Group of Nanoparticle Science and Technology
1 James Bouchier Blvd.
BG-1164 Sofia, Bulgaria
E-mail: nhtd@wmail.chem.uni-sofia.bg

Seichiro Nakabayashi
Department of Chemistry, Faculty of Science
Saitama University
255 Shimo-ohkubo, Saitama City, Saitama
338-8570, Japan
E-mail: sei@chem.saitama-u.ac.jp